Impact of Molecular Clustering on the X-Ray Diffraction Data Analysis for Amorphous Carbon Materials

V. S. NEVEROV[1], A. B. KUKUSHKIN[1] AND V. V. VOLOSHINOV[2]

[1]*National Research Center «Kurchatov Institute», Moscow, Russia*
[2]*Institute for Information Transmission Problems (Kharkevich Institute) of Russian Academy of Science, Moscow, Russia*

ABSTRACT: The impact of molecular clustering on the X-ray diffraction (XRD) diagnostics of amorphous carbon materials is studied on the example of clustering of molecules, including the C60 fullerenes, graphene flakes and diamond-like nanostructures. The clustering is modeled in the frame of the Rigid Body Molecular Dynamics with variable parameter of interaction of atoms in the neighboring rigid molecules. The inverse problem of an amorphous carbonaceous material structural content identification from experimental powder diffraction is formulated as an optimization problem.

1. INTRODUCTION

The identification of structural content of amorphous carbonaceous nanomaterials in the spatial range from few to few tens of nanometers is of practical interest for characterization of carbon nanoparticles in the powder carbon samples, films and various carbonaceous nanomaterials. The X-ray diffraction (XRD) offers a powerful tool to solving this problem. Despite the interpretation of raw data for amorphous materials is a much more complicated task as compared with methods elaborated for the media with the ordered structuring (cf. e.g., [1]), analysis of XRD patterns in the range of scattering wave vector's modulus q from several units to several tens of inverse nanometers, along with the data from other diagnostics, makes it possible to recover the structural content of amorphous carbonaceous nanomaterials (cf., e.g., interpretation [2] of measurements of the synchrotron XRD by hydrocarbon films, deposited in the vacuum vessel of tokamak T-10 in Kurchatov Institute). The success of interpretation to a large extent is determined by the use of comprehensive numerical modeling for solving an inverse problem. The latter, in turn, needs the relevant choice of the physics models for describing the nanostructures, including those peculiar to carbon nanomaterials, the amorphous component of nanomaterials, the interaction of these components at the molecular level, etc. The present paper is aimed at analyzing a particular aspect of the above research program, namely, the impact of molecular clustering on the X-ray diffraction data analysis for amorphous carbon materials in the view of formulating an inverse problem of structural content identification with allowance for these physics effects and for computational feasibility of optimization procedures.

Regarding the status of the above-mentioned research program, we could recall that the interpretation [2] has requested massive calculations of the XRD patterns of multiple carbon nanoparticles of various topology and size. These included the following carbon nanoparticles: fullerenes; carbon nanotubes (CNT) of various radius, chirality and length; axially symmetric ellipsoids (including the spheres); low-aspect-ratio toroids of elliptic cross-section; all possible half-fragments of all above-mentioned structures; various multilayered nanoparticles, including double- to five-wall flakes of the flat graphene, with the flake's position being decorrelated (i.e., glassy graphite). The implementation of the optimization procedure [2] became possible due to using the method [3] of an approximate description of the positions of carbon atoms in a curved graphene sheet. Method [3] is based on the local rearrangement of the neighboring atoms in the walls of hollow carbon $sp2$ structures with graphene-like wall, that enabled us to

calculate the diffraction patters approximately without the knowledge of exact atomic positions in the wall. The method was tested in the case of various carbon nanostructures, including the toroidal CNT [4, 5], and implemented in the XaNSoNS (X-ray and Neutron Scattering on Nanoscale Structures) software package, available for remote use via RESTful web-services created in the Mathcloud (*www.mathcloud.org*) distributed environment. The RESTful web-services can be easily integrated into distributed computing scenarios. Such a scenario of the X-ray diffraction data processing for carbonaceous materials has been presented in [6]. An extension of the algorithm [2] to the case of amorphous carbonaceous material structure identification with a joint X-ray and neutron diffraction data analysis is given in [7].

The developed approach [2,6,7] may be considered as an alternative to the widely used method of the Reverse Monte Carlo (RMC) modeling (cf. e.g., [8]) which assumes the presence of a single (or few) basic building blocks and the spatial homogeneity of the blocks in the sample. The reconstruction is based on the fitting of the experimental Pair Distribution Function of relative atomic positions with that calculated for variable (unknown) structure of basic block(s) and known chemical composition of the sample. In our approach, we allow for the contributions from a very large number of selected basic blocks, including the clustering of basic blocks at spatial scale of interest to nanomaterial fine structuring (~ 1-10 nm). However, the method is very sensitive to computational resources, and one needs a fast-routine calculation at all stages of solving an inverse problem, including the modeling of amorphous molecular clusters with variable main parameters such as intermolecular distance, cluster size and molecule chemical composition.

In the present paper the impact of molecular clustering on the X-ray diffraction (XRD) diagnostics of amorphous materials is studied on the example of clustering of carbon molecules.

For modeling of the clusters we use the Rigid Body Molecular Dynamics method (Sec. 2). We analyze molecular clustering for the C_{60} fullerenes (Sec. 3), graphene flakes and diamond-like nanostructures (Sec. 4). The inverse problem of recovering the structural content of an amorphous carbonaceous material from experimental powder diffraction patterns is formulated as an optimization problem (Sec. 5).

2. THE MODELING OF THE MOLECULAR CLUSTERING

We use the Rigid Body Molecular Dynamics (RBMD) approach [9] to model the carbon molecules clustering. In this approach, molecules are considered as rigid bodies and chemical bond formation and breakage, as well as bond angle change, is prohibited. We use the Lennard-Jones potential to describe the pair interaction between the atoms in the neighboring rigid molecules:

$$U(r_{ij}) = \varepsilon \left[\left(\frac{R_{opt}}{r_{ij}} \right)^{12} - 2 \left(\frac{R_{opt}}{r_{ij}} \right)^{6} \right], \tag{1}$$

where r_{ij} is the distance between the *i*-th and *j*-th atoms of different molecules (relative positions of atoms of the same molecule are strictly fixed), R_{opt} is the minimum point, ε is the potential well depth. The cut-off length is $r_{ij} = 3 R_{opt}$.

The pair potential is unable to describe, e.g., all types of layer stacking in graphite [10], but in our work we are studying the impact of molecular clustering of rigid-body molecules on the diffraction patterns so that we can neglect the effects caused by self-consistent multi-body interaction within molecules. The intermolecular distance in the cluster depends on the R_{opt} parameter and is determined by the minimum of total potential energy which is the double sum of (1) over *i* and *j*.

The steady-state positions of molecules in the sample are found as a stationary solution of the dynamic problem and correspond to the minimum of the total potential energy. To speed up the calculations, we introduced a sink of kinetic energy assuming that the molecules are moving in a viscous medium. Also, we use the quaternion representation to treat the rotation of a rigid body [11]. To reduce the computational time we put all the molecules into a 3D uniform grid, the size of the cell is equal to the cut-off length of the Lennard-Jones potential so that only the atoms within the current and neighboring cells can interact, and there is no need to compute all the distances r_{ij}. The time

integration is performed in the following order: grid update, force calculation, angular and linear momentum update, quaternion update, relative atomic positions and center of the mass position update, grid update. The created numerical code is parallelized using the MPI.

3. CLUSTERING OF THE C_{60} FULLERENES

Here we consider crystal and amorphous clusters of the C_{60} fullerenes. Crystal state of C_{60} fullerene (fullerite) has the face-centered cubic (FCC) lattice with the period $a = 14.2$ Å. The distance between the centers of neighboring molecules is equal to 10 Å, and the distance between the closest atoms of neighboring molecules is about 3 Å. Crystal cluster of C_{60} is shown in Figure 1a.
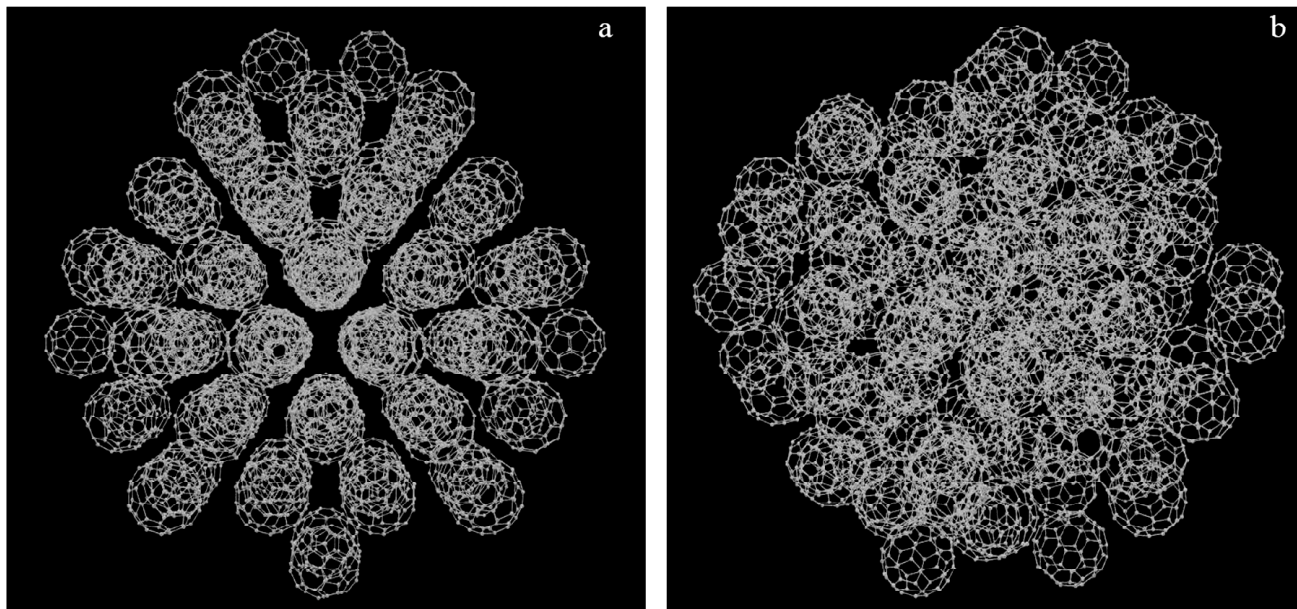
Figure 1: **(a) Crystal cluster (fullerite) of 104 C_{60} fullerenes of size D ~ 54-60 Å, (b) amorphous cluster of 112 C_{60} fullerenes of nearly the same size, calculated using the RBMD with Lennard-Jones potentials (1) for R_{opt} = 3.5 Å**
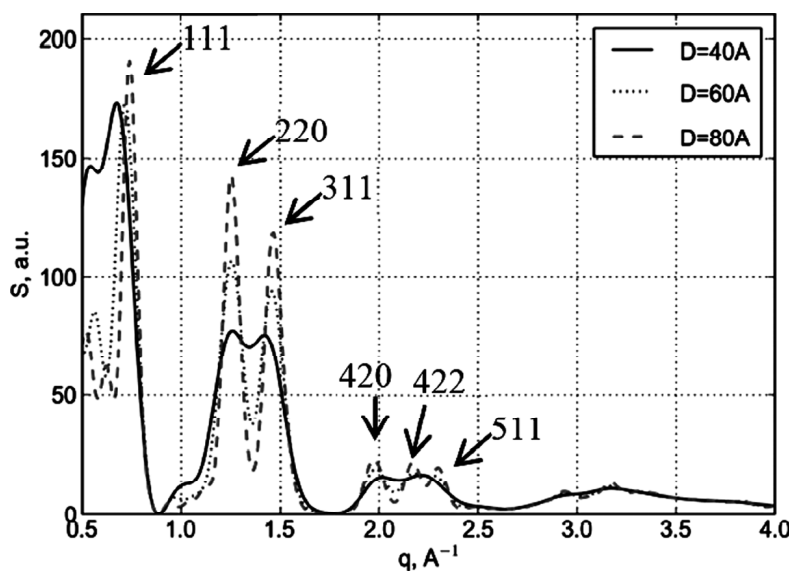

Figure 2: **Calculated XRD patterns of crystal C_{60} clusters (see Fig. 1a) of different size. All the XRD patterns are normalized to the total number of atoms in the structure**

Figure 2 shows how the size of the cluster changes the calculated XRD patterns. Hereinafter all the XRD patterns are normalized to the total number of atoms in the structure. The polarization factor which depends on scattering angle is omitted to make it possible to plot the intensity as a function of a single argument, the scattering vector modulus, $q = /\mathbf{k} - \mathbf{k_0}/$, where $\mathbf{k_0}$ and $\mathbf{k}$ are the incident and scattered wave vectors, and not of the scattering angle. Figure 2 shows strong dependence of the shape of the diffraction peaks on the size of the crystallite at $q < 2.5$ Å^{-1}. The XRD patterns of all clusters are almost identical at $q > 2.5$ Å^{-1} because in this range the patterns would depend on the mutual orientation of fullerenes in the cluster while in our case the latter was set random. Such a randomness may be caused by the thermal rotation of molecules that will not occur only at low temperatures. The strong dependence of the XRD patterns on the crystallite size makes it possible to determine the latter in the sample even if the crystallite size is about few nanometers.

The amorphous C_{60} clusters are modelled using the RBMD approach outlined above. The initial positions and spatial orientations of molecules were set random. An example of the resulting amorphous C_{60} cluster is shown in Figure 1b. Unlike the crystallite, in the amorphous cluster the distance between molecules could vary, so that the clusters with three values of R_{opt} parameter: $R_{opt} = 3.0$ Å, $R_{opt} = 3.5$ Å and $R_{opt} = 4$ Å cover the range of interest. The calculated XRD patterns of these clusters of the size $D = 60$ Å and of C_{60} crystallite of same size are shown in Figure 3. It is seen that the phase state (crystal or amorphous) of the C_{60} sample can be identified due to the "splitting" of the wide peak at $q = 1.3$ Å^{-1} in the amorphous state into the 220 and 311 FCC lattice peaks in the crystal state. The peak at $q = 0.75$ Å^{-1} s is also determined by the intermolecular distance, and it exists in the amorphous state despite there is no FCC lattice. The dependence of XRD pattern on the R_{opt} parameter is strongest at $q < 1.5$ Å^{-1}.
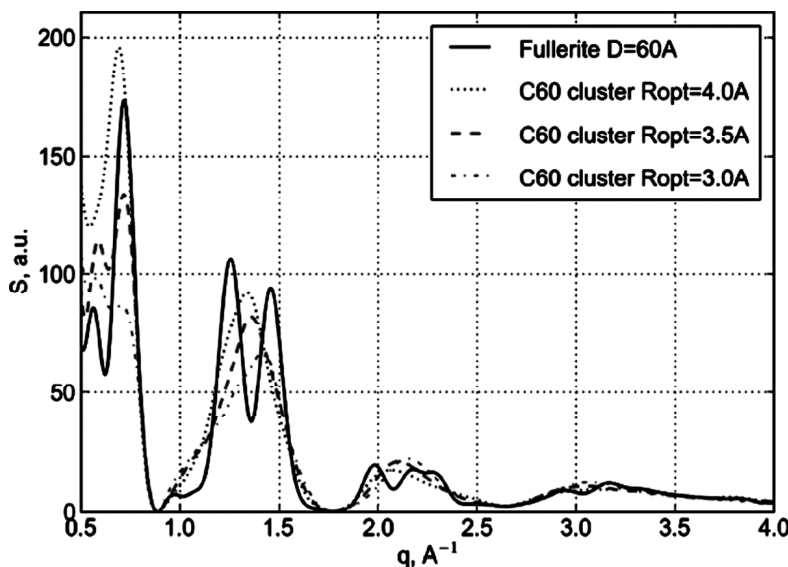

Figure 3: Calculated XRD patterns of amorphous C_{60} clusters modeled by RBMD with potential (1) with R_{opt} parameters equal to: 3.0 Å, 3.5 Å and 4 Å and of crystal C_{60} cluster. All clusters have the same size, ~ 60 Å

The position of 0.75 Å^{-1} peak varies in the range of 0.7-0.8 Å^{-1} while its height also depends on R_{opt}. The position of this peak is closest to that of the FCC 111 peak when $R_{opt} = 3.5$ Å. This means that intermolecular distance of 10 Å in the crystallite corresponds to this value of R_{opt}.

Figure 4 shows the dependence of the calculated XRD patterns on the size of amorphous C_{60} cluster. This dependence is very weak at $q > 0.8$ Å^{-1} so that all the XRD patterns are almost identical in this region. The difference of curves is seen in the shape of the peaks at 0.75 Å^{-1} but even here the dependence becomes weaker with increasing size of the cluster. This makes almost impossible to determine the size of amorphous C_{60} cluster in the sample from the measured wide angle XRD pattern.
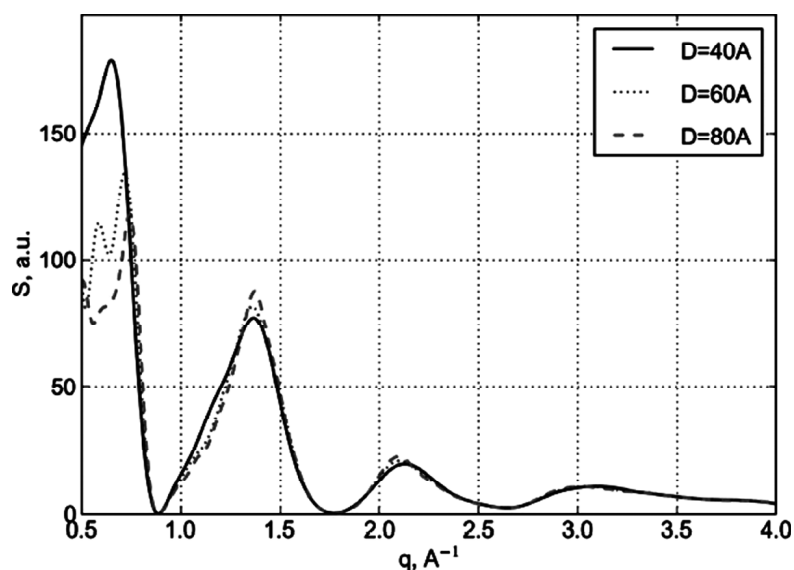
Figure 4: Calculated XRD patterns of amorphous C$_{60}$ clusters of different size, modeled by the RBMD with potential (1) for R_{opt} = 3.5 Å

The real samples may contain both crystal and amorphous clusters. The modeling of such clusters with various parameters (such as intermolecular distance, for amorphous state, or the size, for crystal state) and calculations of the XRD patterns make it possible to determine some parameters (e.g., crystal cluster size, the ratio of molecules in crystal/amorphous state, intermolecular distance) of the structural content of the sample. The inverse problem to determine the structural content of the sample by analyzing the experimental XRD patterns is formulated in section 5 of the paper.

4. CARBON *sp*2 AND *sp*3 CLUSTERS

Another typical problem for carbon amorphous materials is determination of the parameters of clusters of the *sp*2 and *sp*3 hybridized atoms as well as determination of the respective ratio of *sp*2/*sp*3. The Auger electron spectroscopy, electron energy loss (EELS) and near edge X-ray absorption fine structure (NEXAFS) spectroscopies are frequently used for solving this problem. Although these methods are good for determining the *sp*2/*sp*3 ratio they do not provide information about cluster sizes and shapes. Here we consider the clustering of small (about 40 atoms) building blocks (molecules) of the *sp*2 (graphene-like) and *sp*3 (diamond-like) structure, using the RBMD method of section 2.
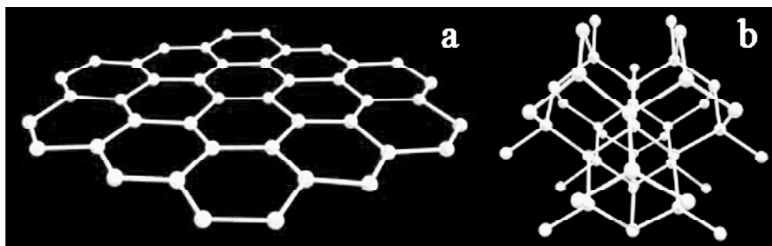

FIgure 5: (a) Graphene flake (43 atoms), (b) diamond-like *sp*3 structure (45 atoms)

Figure 5 shows the building blocks for the clusters: graphene flakes (43 atoms) and diamond-like *sp*3 structures (45 atoms). The XRD patterns of graphene flake and diamond-like structure are shown in Figure 6. The peak at $q = 1.5$ Å^{-1} produced by scattering on the diamond-like structure pattern is caused by the finite size of the structure. All other peaks produced by both structures are caused by the layout of atoms in the structure. Their height and sharpness increase with increasing size of these blocks. We chose the blocks of such a small size just to demonstrate
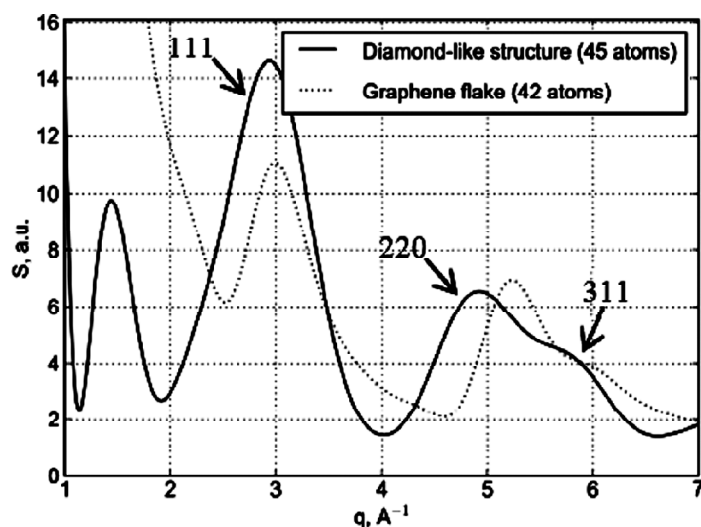
Figure 6: Calculated XRD patterns of single graphene flake and diamond-like *sp*3 structure (see Fig. 5)

the complexity of XRD analysis for amorphous materials. As seen in Figure 6, additional complexity appears because the peak at $q = 3$ Å^{-1} is present on both patterns, and the difference between the centers of the peaks at $q = 5$ Å^{-1} on the *sp*2 and *sp*3 XRD patterns is less than 0.5 Å^{-1}.

To analyze the dependence of XRD pattern on the number of carbon atoms in the *sp*2 and *sp*3 states in the samples we modeled large clusters of 25200 atoms containing the graphene flakes and the diamond-like structures in various proportions. The flakes and diamond-like structures were considered as rigid bodies and potential (1) was used as in the previous section for C_{60} molecules. We chose $R_{opt} = 3.5$ Å for both blocks. The initial positions and spatial orientations of blocks were set random. One of the resulting clusters containing the 30% of atoms in the *sp*2 hybridization state (graphene flakes), and the 70% of atoms in the *sp*3 hybridization state, is shown in Fig. 7.
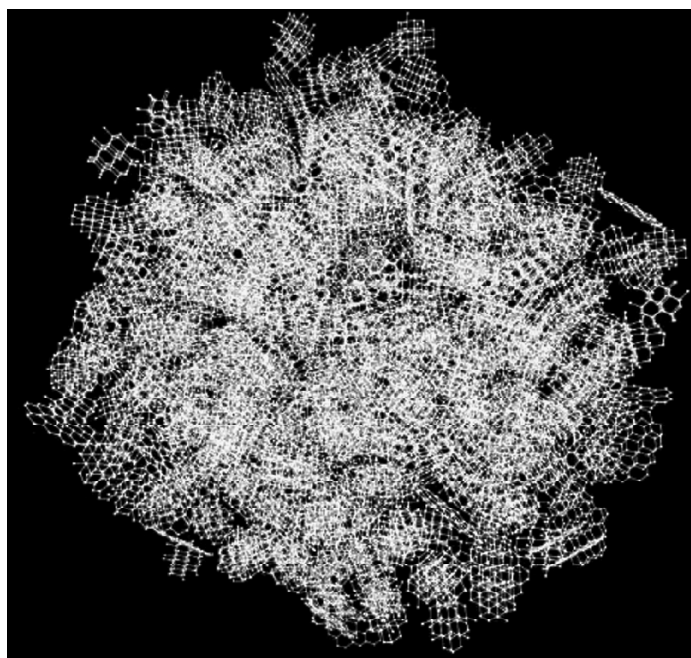

Figure 7: The cluster of 25200 carbon atoms calculated by RBMD with potential (1) with $R_{opt} = 3.5$ Å containing the 30% of atoms in the *sp*2 hybridization state (graphene flakes), and the 70% of atoms in the *sp*3 hybridization state (diamond-like structures) (see. Fig. 5).

Figure 8 shows the dependence of the calculated XRD patterns on the $sp2/sp3$ hybridization ratio in the modeled amorphous clusters. The dependence is weak at $q > 2.5$ Å^{-1}, and the position of the center of the peak at $q = 3$ Å^{-1} slightly shifts to the left for $sp3/sp2 > 1$. The most significant difference takes place at $q < 2.5$ Å^{-1}. When the graphene flakes dominate, the intense peak at $q = 2$ Å^{-1} appears as a result of graphitization, i.e., parallel spatial orientation of the neighboring graphene flakes. This peak corresponds to the interplanar spacing of 3.14 Å, close to that in graphite (3.35 Å). When the diamond-like $sp3$ structures dominate, the peak at $q = 1.5$ Å^{-1} appears that is caused, as mentioned above, by the finite size of the $sp3$ structure.
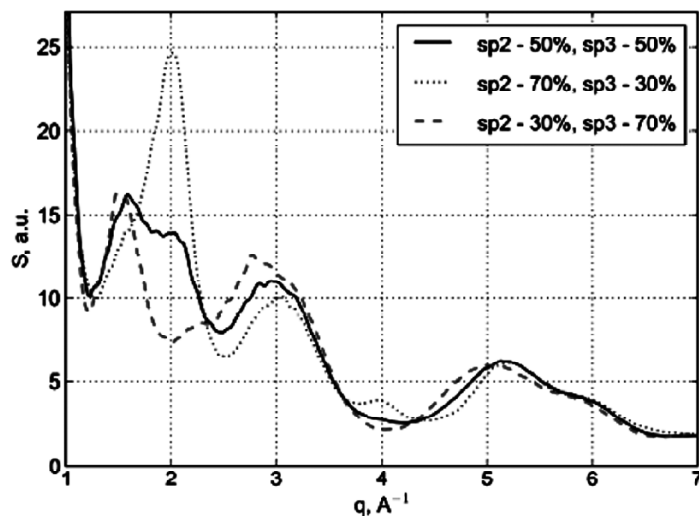

Figure 8: **Calculated XRD patterns of clusters of 25200 carbon atoms (see Fig. 7) with different number of atoms in the $sp2$ and $sp3$ hybridization state**
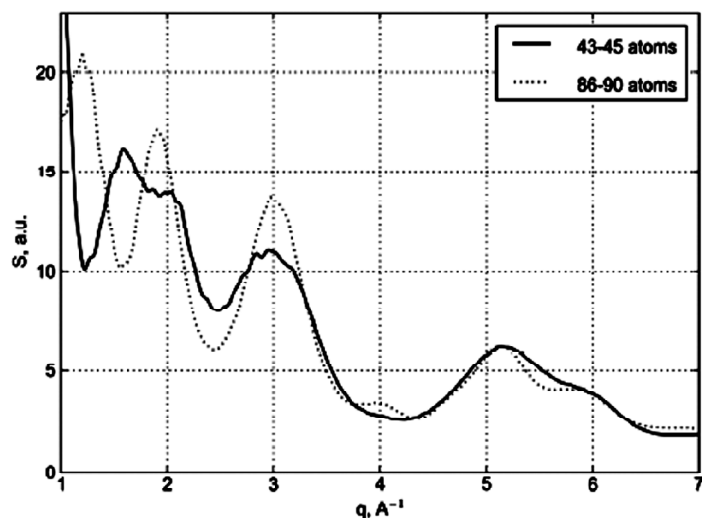

Figure 9: **Calculated XRD patterns of clusters of carbon atoms containing the 50% of the $sp2$ (graphene flakes) and 50% of the $sp3$ (diamond-like structures) blocks of different size. The number of atoms in the block is indicated in the legend**

The real samples may contain the $sp2$ and $sp3$ blocks of different sizes and shapes. Both the size and shape could be a variable parameter of modeling. Here we analyze the dependence of XRD pattern on the block size only. We modeled the cluster similar to one shown in Figure 7 but consisting of the blocks of the doubled number of atoms (86 atoms for graphene flakes and 90 atoms for diamond-like structure). Figure 9 shows three major changes of the XRD patterns caused by the increasing size of blocks. First and second, there is a distinct increase of the

height and sharpness of the peaks at $q = 2$ and $3\,\text{Å}^{-1}$. Third, the peak at $q = 1.5\,\text{Å}^{-1}$ related to the size of $sp3$ cluster, moves to $q = 1.5\,\text{Å}^{-1}$ that is directly caused by the increase of structure size. The dependence of XRD patterns on the $sp2/sp3$ ratio and the size and shape of blocks makes it possible to determine the structural content of the mixed $sp2/sp3$ samples. The corresponding inverse problem is formulated in the next section.

5. THE INVERSE PROBLEM FOR THE STRUCTURAL CONTENT OF AN AMORPHOUS CARBONACEOUS MATERIAL

The inverse problem of recovering the structural content of an amorphous carbonaceous material from experimental powder diffraction patterns was formulated in [2]. The algorithm [2] assumes the knowledge of chemical composition of the sample and is valid for a known structural content of impurities. For instance, in particular case of application to the hydrocarbon films from tokamak T-10 [2], the latter means that the impurities (e.g., small amount of heavy atom metals) were present only as separate atoms. Here we generalize our approach to the case of amorphous materials where the structural content of *all* components, including the impurities, in contrast to chemical composition of the sample, is not known and should be recovered from the experimental data.

The respective optimization problem is the minimization of the norm of the vector, each element of which represents the difference between the experimental powder XRD pattern and the model X-ray scattering intensity at the current point of discrete finite set of the values of the scattering vector modulus q. The dimension of this "discrepancy vector" equals to the total number of points in the experimental data. The model intensity is calculated as a sum over the calculated XRD patterns of all selected nanostructures with unknown weight coefficients. The structure is meant as a certain atomic ensemble with fixed parameters. The unknown constant background also should be included in the model XRD intensity. The formula for the vector element is as follows:

$$Z_j(\mathbf{x}, b) \equiv S_{\text{exp}}(q_j) - \sum_{i=1}^{N} S_i(q_j) x_i - b \qquad (j = 1:m), \tag{2}$$

where $S_{\text{exp}}(q_j)$ is an experimental powder XRD pattern; $S_i(q_j)$ is a calculated XRD pattern for the i-th structure normalized to the number of atoms in the structure; j is the number of the current point in the discrete space of scattering vector modulus q; N is the total number of selected structures; m is the total number of points in the experimental data. The unknown parameters are the weight coefficients x_i and the constant background b. The weight coefficient x_i is proportional to the fraction of the i-th structure in the sample, it also involves the unknown ratio of the arbitrary units of experimental and calculated XRD patterns. The above fraction is equal to the ratio x_i/X, where X is a sum of all x_i:

$$\sum_{i=1}^{N} x_i \equiv X. \tag{3}$$

There are three additional constraints on the unknown parameters:

$$x_i \geq 0 \qquad (i = 1:N), \tag{4}$$

$$B_{\text{min}} \leq b \leq B_{\text{max}}, \tag{5}$$

$$W_{\text{min}}^{el} X \leq \sum_{i=1}^{N} w_i^{el} x_i \leq W_{\text{max}}^{el} X \qquad (el = 1:M). \tag{6}$$

where the latter condition describes the bounds for the chemical composition of an *optimal* structure ensemble, i.e. found via solving an inverse problem, around the known chemical composition of the sample; B_{min} and B_{max} are the lower and upper bounds for the unknown constant background in the experimental data; w_i^{el} is the known fraction of chemical element el in the total number of atoms in the i-th structure; M is the total number of chemical elements in

the sample; $W_{\min}^{el}$ and $W_{\max}^{el}$ are related to the known chemical composition of the sample as follows. As far as the fraction of chemical element el in the sample is known with some error, one has $W_{\min}^{el} = W^{el} - Err$, $W_{\max}^{el} = W^{el} + Err$. If the chemical composition of the sample is known with a high accuracy, and the Err value is negligible, the inequality (6) transforms into the equation:

$$\sum_{i=1}^{N} w_i^{el} x_i = W^{el} X \qquad (el = 1 : M).\qquad(6.1)$$

The constraint (6) allows us to take into account the contribution from the non-carbon nanostructures, or nanostructures of mixed chemical composition, in the same way as from carbon nanostructures. As far as now the structural content of non-carbon structures is not known, their contribution to the scattering intensity is not merely an unknown background like in [2].

Statistical characteristics of experimental data errors may be unknown, therefore we propose to consider various norms of the vector (2) which are to be minimized. Similarly to [2], one can use the following three versions of minimization:

$$\sum_{j=1}^{m} |Z_j(\mathbf{x}, b)| \xrightarrow{\mathbf{x}, b} \min \quad (L_1 \text{ norm}),\qquad(7)$$

$$\sum_{j=1}^{m} (Z_j(\mathbf{x}, b))^2 \xrightarrow{\mathbf{x}, b} \min \quad (L_2 \text{ Euclidean norm}),\qquad(8)$$

$$\max_{j=1:m} |Z_j(\mathbf{x}, b)| \xrightarrow{\mathbf{x}, b} \min \quad (L_\infty \text{ norm}).\qquad(9)$$

The comparison of the results of minimization of three different norms provides an additional control of the accuracy of solving the inverse problem.

One can see that the proposed method of recovering the structural content of an amorphous material allows for concurrent computation of different structures (e.g., using the RBMD method described above) and their XRD patterns. So the proposed method is friendly to the distributed computing. Moreover, three optimization problems mentioned above are independent and may be solved in parallel.

6. CONCLUSIONS

A method for numerical modeling of clustering of carbon molecules is proposed for the problem of the X-ray diffraction (XRD) diagnostics of a wide class of carbon amorphous materials. This method uses the formalism of the Rigid Body Molecular Dynamics (RBMD) with the Lennard-Jones potentials for the pair interaction between the atoms in the neighboring rigid molecules.

The method is applied to analysis of clustering of the following molecules: C_{60} fullerenes, $sp2$-hybridized (graphene flakes) and $sp3$-hybridized (diamond-like) nanostructures. The dependence of XRD patterns of amorphous cluster on the intermolecular distance is analyzed. The following particular results are obtained. The XRD patterns for crystal and amorphous C_{60} clusters differ significantly if the size of the clusters exceeds 40 Å. The XRD patterns of the graphene flakes and diamond-like nanostructures of few tens of atoms show strong dependence on the block's size and the $sp2/sp3$ ratio in the sample. The difference between the XRD patterns is significant even for the very small blocks, of 40-50 atoms.

The previously formulated inverse problem of recovering the structural content of an amorphous carbonaceous material from experimental powder XRD patterns is generalized to the case of amorphous materials where the structural content of all components including the impurities, in contrast to chemical composition in the sample, is

not known and should be recovered from the experimental data. The proposed method of the XRD pattern analysis is friendly to the distributed computing.

Acknowledgments

References

[1]   S. J. L. Billinge, and I. Levin, *Science*, **316**, (2007), 561.

[2]   A. B. Kukushkin, V. S. Neverov, N. L. Marusov, I. B. Semenov, B. N. Kolbasov, V. V. Voloshinov, A. P. Afanasiev, A. S. Tarasov, V. G. Stankevich, N. Yu. Svechnikov, A. A. Veligzhanin, Ya. V. Zubavichus and L. A. Chernozatonskii, *Chem. Phys. Lett.*, **506**, (2011), 265-268.

[3]   L. A. Chernozatonskii, V. S. Neverov, and A. B. Kukushkin, A Calculation Model for X-Ray Diffraction by Curved-Graphene Nanoparticles, *Phys. B: Cond. Matter*, **407**, (2012), 3467-3471.

[4]   L. A. Chernozatonskii, *Phys. Lett.*, **A-170**, (1992), 37.

[5]   E. G. Gal'pern, I. V. Stankevich, A. L. Chistyakov, and L. A. Chernozatonskii. Fullerenes, Nanotubes, *Carbon Nanostr*, **2**(1), (2007), 1.

[6]   V. V. Voloshinov, and V. S. Neverov. X-Ray Diffraction Data Processing for Nanomaterials in the Distributed Environment of RESTful Services, *Information Technology and Computation Systems (in Russian)*, **4**, (2011), 10-20.

[7]   V. S. Neverov, V. V. Voloshinov, A. B. Kukushkin, and A. S. Tarasov, Algorithm of Amorphous Carbonaceous Nanomaterial Structure Identification with a Joint X-Ray and Neutron Diffraction Data Analysis, Preprint arXiv:1301.3418 [*cond-mat.mtrl-sci*] (2013), 9 pages,

[8]   R. L. McGreevy, Reverse Monte Carlo Modelling, *J. Phys. Condens. Matter*, **13**, (2001), R877.

[9]   G. Ciccotti, and J. P. Ryckaert, Molecular Dynamics Simulation of Rigid Molecules, *Computer Physics Reports*, **4**(6), (1986), 346-392.

[10] A. Ito, and H. Nakamura, *Commun. Comput. Phys.*, **4**, (2008)**,** 592-610.

[11] D. C. Rapaport, Molecular Dynamics Simulation Using Quaternions, *J. Comp. Phys.*, **60**, (1985), 306314.